Turkish Journal of Electrical Engineering & Computer Sciences

http://journals.tubitak.gov.tr/elektrik/

Research Article

Turk J Elec Eng & Comp Sci
(2023) 31: 693 – 705

doi:10.55730/1300-0632.4011

Well-conditioned T-matrix formulation for scattering by a dielectric obstacle

Murat Enes HATİPOĞLU, Fatih DİKMEN*
Department of Electronics Engineering, Faculty of Engineering, Gebze Technical University, Kocaeli, Turkey

Received: 08.11.2022 • **Accepted/Published Online:** 17.05.2023 • **Final Version:** 28.07.2023

Abstract: The classic formulation of the extended boundary condition method is revisited to inject the regularization operators for the unknown coefficients of the eigen-function expansions for the travelling and standing waves throughout the dielectric scatterer. It is shown that, using the new definitions, the existing algorithm of the scattering field calculation can be kept the same for its well-conditioned version. This is exemplified for scalar 2D problems for both TM and TE polarization under illumination of a line source. The condition numbers of the matrix operators in the new version of the algorithm are drastically reduced when the regularization interfaces are eigen-surfaces of the field expansions, i.e. circles on extended boundaries in the counter null-fields. The arbitrariness of the boundary interface is involved in the calculations, via parameterized contours and effects of elongation and corrugation of the interface boundary contour on the condition of the algorithm is extensively discussed in comparison with the results of the boundary integral equation formulation of the same problem.

Key words: T-matrix, dielectric scatterer, regularization

1. Introduction

The T-matrix method is an indispensable instrument in the multiple scattering calculations within a wide range of scientific research from nano-technology to astrophysics. Its applications to the novel scattering problems [1]–[3] are disseminated so frequently that the comprehensive thematic T-matrix reference database was regularly updated [4] as a tradition kept by Mishchenko. This tradition may have sadly come to an end after the last update [5] as he passed away according to [4].

The theoretical ground of the method is based on the extinction theorem which is formulated with one of the two outcomes of the surface equivalence principle [6, 7]. This principle formulates the fields satisfying homogeneous Helmholtz equations in the homogeneous regions of the free space separated with a smooth boundary whereas these fields also satisfy certain boundary conditions on. While the equivalent surface current densities on the boundary are the source of the scattering field in the region on one side of the boundary, these densities extinguish the fields on the other side causing null-fields in this region.

It would not be unfair to state that the engineering with the latter outcome of the surface equivalence principle i.e. the null-field methods applied to scattering and radiation of not only electromagnetic waves but also waves of various origins such as elastic or acoustic waves [8, 9] are performed with a more specific tuning and variations than the former outcome of the surface equivalence principle: the boundary element methods (BEM) or boundary integral equation (BIE) methods [10, 11] which are more universal than the latter. For the same variety of applications, the establishment of a vast variety of direct solutions on the object boundary

*Correspondence: dikmen@gtu.edu.tr

in applications drives the modern software on electromagnetic engineering rendering the BEM or BIE methods to be more widespread currently [12]. But the null-field methods are in continuous demand in the particular important scope of applications. Even more, they formed establishment of multiple scattering mechanisms consisting of open boundaries, isolated T-matrices of which exploited concepts in BIE formulations [13].

The T-matrix method which is also called extended boundary condition (EBC) method as one of the null-field methods extends the boundary to a surface in the null-field region that can be one of the eigen-surfaces of the proper separable coordinates with respect to the homogenous Helmholtz equation. Beyond these eigen-surfaces in the null-field region, the eigen-function expansions of the unknown surface currents on the arbitrarily shaped scatterer boundary are found valid as long as it is not elongated or corrugated. The generalized multipole method [14] and method of auxiliary sources [15] are the other two methods that do not pronounce such a limitation which are also based on extinction theorem. They trace the unknown coefficients of the eigen-function expansions of the point sources in the null-field interspersed along the boundary. They may arrange the types and amplitudes of the expansions as well as the locations of the point sources in due process of satisfying the boundary condition. The null-field integral representations can further be exploited to form relevant BIE formulations [7, 16]. The main concern of these applications is efficient scattering formulations when the boundary is quite arbitrary. The T-matrix method on the other hand is functional for scattering of waves from a multitude of objects with one type of eigen-function expansion for all [17]. In this study, we elaborate on the well-conditioned version of this algorithm for an isolated dielectric scatterer specified to cylindrical targets with arbitrary cross sections, to form a background for further calculations regarding multitudes of them.

There are two aspects of the ill-conditioning regarding the T-matrix method first of which is geometrical. The less the deviation of the scatterer surface from the eigen-surface that the eigen-expansions of which is used in calculations, the less the ill-conditioning [7]. The second aspect of the ill-conditioning occurs even when the surface is an eigen-surface due to the eigen-function expansions used i.e. a circle/sphere in 2/3 dimensions. Especially when the radial eigen-functions e.g., Bessel and Hankel functions of integer/half-integer indices for 2/3 dimensional problems in case the cylindrical/spherical harmonic expansions are used, the unknown coefficients possess fast decay and growth with respect to the truncation numbers [18]. This feature of the unknowns is a threat known as "numerical catastrophe" to the accuracy in the computer with finite precision where doubling the precision can only shift it to higher truncation numbers [22]. It is observed to prevent the expression of the resonant content of the obtained solutions in [19]. The regularization of this feature has been of critical importance especially when the interaction between more than one boundaries has to be formulated with linear algebraic equation systems (LAES) in the computer with an algorithm that avoids the round-off errors during matrix inversions [20]. Although the awareness on this second aspect has a history about four decades, we witness that the advent of the computer hardware allowing more precision in calculations is leaving it behind. Nevertheless we can find works on resolving the stability and condition of specific problems every now and then [21]. Here we have thoroughly aim to exemplify the positive impact of the novel regularization scheme about to be suggested, even when we do not dwell on the multiple scatterers.

In this study, we suggest a novel regularization to the T-matrix method of scattering by an arbitrarily shaped dielectric boundary that is applicable for the multiple scattering calculations including the recursive ones on their existing scheme of application. We use the outcomes from the formalism of the analytical regularization method (ARM) [22], that establishes the left and right hand side regularizer pairs of an operator which can be of integral, integro-differential or matrix type that leads to an ill-conditioned LAES (LAES_i) in order to transform

the operation into a well-conditioned LAES (LAES_w). The ARM is usually defined on BIE formulations, but its version coinciding with null-field methods in [23] involves eigen-function solutions of dielectric scatterers, boundaries of which are circles. The use of the left and right hand regularizer pairs for the eigen-surface scattering problem there is shown to mend the numerical stability and the conditioning problems encountered before their employment. In subsection 2.2 we expand on this for the formulation we cover here. We discuss the results of employing the regularization developed for eigen-surface scatterers on the eigen-surfaces on extended boundaries in T-matrix formulations. But before that we review the T-matrix method in the formalism presented in [7] in the next section. Then the numerical results on several cases reporting the well-condition of the presented algorithm follow before the conclusion.

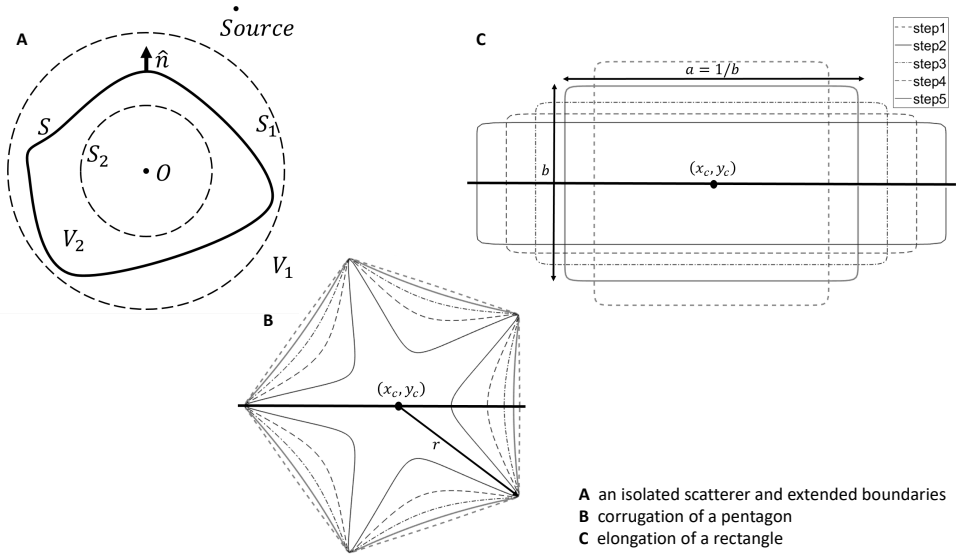

Figure 1. The isolated scatterer configuration and sample scenarios with a pentagon and a rectangle.

2. Formulation

2.1. The T-matrix method for an isolated scatterer

We shortly review the version of the extended boundary condition (EBC) method presented in [7] for our convenience in establishing the conceptual framework and refer the reader there for detailed formulation. It is based on the surface integral representation (SIR) of the scattering fields ($\phi_{sca}(\mathbf{r})$) from a dielectric obstacle (Figure 1A) of the $e^{-j\omega t}$ -time harmonic scalar waves incident in the unbounded region V_1 ($\phi_{inc}(\mathbf{r})$). $\phi_{sca}(\mathbf{r})$ satisfies the homogeneous Helmholtz equation in the regions $V_i, i = 1,2$ with the equivalent integral representations on the interface separating them (null-field region index is $\imath_i = i + (-1)^{(i-1)} = 2,1$ in terms of nonnull-field region index $i = 1,2$):

$$\phi_{sca}(\mathbf{r}) = (-1)^{i+k+1} \int_S dS' \hat{n}' \cdot \left[g_i(\mathbf{r},\mathbf{r}') \nabla' \phi_i(\mathbf{r}') - \phi_i(\mathbf{r}') \nabla' g_i(\mathbf{r},\mathbf{r}') \right] = \begin{cases} \phi_i(\mathbf{r}) & -\delta_{i,k}\phi_{inc}(\mathbf{r}); \quad \mathbf{r} \in V_i \\ 0 & -\delta_{i,k}\phi_{inc}(\mathbf{r}); \quad \mathbf{r} \in V_{\imath_i} \end{cases}. \quad (1)$$

Here $\delta_{i,k}$ is Kronecker's delta, used to distinguish the region of the incident field with the region index $k \in 1,2$ as $k = 1$ in the scenario in Figure 1A and so forth unless indicated. $g_i(\mathbf{r},\mathbf{r}'), i = 1,2$ is the free space Green's

function of the scalar Helmholtz equation dimensional specification of which is not required at this stage. Left hand side of (1) has two variants: (i) The variant for $r \in V_i$ implies that the scattering field in the region is radiated by surface sources $\varpi_i^{\pm}(\mathbf{r}')$, ($\pm$ regard to the function spaces they belong on S which will help us below).

$$\varpi_i^{-}(\mathbf{r}') = \hat{n} \cdot \nabla' \phi_i(\mathbf{r}') \quad \text{and} \quad \varpi_i^{+}(\mathbf{r}') = \phi_i(\mathbf{r}') \qquad i = 1,2; \quad \mathbf{r}' \in S \tag{2}$$

In this variant, the SIR can be further elaborated to lead to the boundary integral equation (BIE) formulations with observation of (1) on S. (ii) The variant for $\mathbf{r} \in V_{i_i}$, implies that these surface sources on S nullify the total fields in the corresponding regions proving the extinction theorem. This is the basis for the EBC method (also known as the null-field method or the T-matrix method) and its solution is obtained with two null-field equations in each region under the following pair of boundary conditions to determine the four unknown surface source functions exhibited in (2),

$$\phi_1(\mathbf{r}) = \phi_2(\mathbf{r}) \quad \text{and} \quad p_1 \hat{n} \cdot \nabla' \phi_1(\mathbf{r}') = p_2 \hat{n} \cdot \nabla \phi_2(\mathbf{r}) \quad \mathbf{r} \in S, \tag{3}$$

where $p_i, i = 1,2$ are media parameters specified according to the field sought for.

The method is called T-matrix method especially because it is possible to express the unknown coefficients of the scattering field from an isolated obstacle by a matrix called T-matrix, multiplied with the coefficients of the incoming wave eigen-functions of the incident field. This enables the validity of the solution for varying excitations with no necessity to reproduce the T-matrix again which is a feature unlikely to achieve with the BIE formulations mentioned in (i) above. We owe this flexibility to the following two assumptions: (i) We observe the null-fields (1) in regions V_{i_i} $(i = 1,2)$ (Figure 1A) extending the region V_i to the eigen-surfaces (sphere-3D, circle-2D) S_{i_i} away from S, in combination with boundary conditions (3) written in the SIRs on S. (ii) We expand the unknown surface sources nullifying the total field beyond S_{i_i} to the corresponding eigen-functions of the eigen-surfaces in V_{i_i} as well as the Green function and the incident field.

As the incident field with the known eigen-function coefficient vector $\mathbf{a}$ impinges on the boundary of the isolated scaterrer S from V_i, the eigen-function coefficient vectors $\boldsymbol{\alpha}$ and $\mathbf{f}$ of transmitted field to V_{i_i} and the reflected field to V_i respectively remain to be determined for any choice of the value of the incident field index $k \in 1,2$. The isolated scatterer inverted matrices and the condition of these inversions are of concern in this study regarding the T-matrix relations $\boldsymbol{\alpha} = -i\overline{\mathbf{Q}}^{-1} \cdot \mathbf{a}$ and $\mathbf{f} = \overline{\mathbf{T}} \cdot \mathbf{a}$ that define these coefficients through the incident field data. We can specify $k = 1$ as in the case in Figure 1A (-or $k = 2$ if the incident field is a travelling from inside out). Note that $\hat{n}$ has to point to the region where the source of the incident field is. The matrix $\overline{\mathbf{Q}}$ is calculated in this case, as the outcome of the extinction theorem in (1) and the boundary conditions (3) combined, expanding the unknowns into standing (-travelling) wave eigen-function series (see Appendix). After this, the T-matrix is determined as $\overline{\mathbf{T}} = -\mathfrak{Re}\overline{\mathbf{Q}} \cdot \overline{\mathbf{Q}}^{-1}$ from the relation of the SIR of $\phi_{sca}(\mathbf{r})$ (1) and its travelling (-standing) wave eigen-function series. $\mathfrak{Re}\overline{\mathbf{Q}}$, is the "Regular Part" of $\overline{\mathbf{Q}}$ which is the matrix where the radial travelling wave functions in $\overline{\mathbf{Q}}$ are converted to the radial standing wave functions. Conventionally the matrix used for the reflected field coefficients of the isolated scatterer ($\mathbf{f}$) is called the "T-matrix" but both coefficients involve the inverse of the same matrix, i.e. $\overline{\mathbf{Q}}^{-1}$ and it suffices to choose one of the unknowns to scrutinize the condition of the algorithm.

2.2. The well-conditioned T-matrix method

It is the fact with T-matrices that they are ill-conditioned matrices as the shape of S deviates at a high amount from the eigen-surface's, with corrugation or elongation of S. It means that, as the scatterer geometry allows the eigen-function expansion of the scattered fields, this flexible method is in demand. This occurs when the shell formed by EBC surfaces S_{ι_i} is thin enough (Figure 1A).

Aside from that geometrical condition, the numerical condition of the matrix inversions involved in solving the recursive or the nonrecursive implementations of the T-matrix algorithm has been of concern in the past [18]. The normalization of the scattering field coefficients can provide a finite static limit [25] or provide a factorization maintaining the resonance content [19] from the solutions. To address this issue in the T-matrix method's context we need to recall the Rayleigh method which leads to the same T-matrix formulation by a reasoning other than the EBC [7]: The boundary conditions (3) are enforced on S using the standing/travelling wave eigen-function expansions for the $<$ transmitted & incident $>/<$ reflected $>$ fields in relevant regions. Elimination of the unknown reflected field coefficients from the resulting equation system by i) testing with transmitted/reflected wave eigen-functions and their normal derivatives, ii) integrating over S, leads to the same isolated scatterer T-matrices.

The thickness of the abovementioned shell is zero ($S_1 = S_2 = S$), if the scatterer boundary is an eigen-surface (sphere 3D/circle 2D) of a specified radius – a. Let us consider the eigen-function expansions of the $\phi_{sca}(\mathbf{r})$ as well as the SIR they are equal to in (1) then. We can assume the surface harmonic – SH - (spherical 3D/Fourier 2D harmonics) expansion of the unknown sources in (2) and consider them in (1). Recall that the eigen-function expansion of the Green's function via addition theorem is a definition of its SHs too. Having substituted these expansions in the SIR of the $\phi_{sca}(\mathbf{r})$ in each region $V_i, i=1,2$, we can expose the form of its eigen-function expansion coefficients in Rayleigh method [24]. This reveals the dependence of the unknown eigen-function coefficients to the SH coefficients of the unknowns (2) multiplied by the SH coefficients of the Green's function on S owing to the orthogonality of the SHs on S.

To exemplify this we give the following result achieved in 2D [23],

$$\lambda_m^i = \frac{j\pi}{2}\left[\varpi_{i,m}^- W_m^{(\iota_i)}(k_i a) - k_i \varpi_{i,m}^+ W_m^{(\iota_i)'}(k_i a)\right]. \tag{4}$$

Here, λ_m^i are coefficients of the eigenfunction expansions $\phi_{sca}(\mathbf{r})$ in each region $V_i, i=1,2$. $\varpi_i^{\pm}$ are Fourier coefficients of the nature $\varpi_i^{\pm}(\mathbf{r}') \in H^{\pm 1/2}(S)$ (2) where $H^{\pm 1/2}(S)$ are the pair of Sobolev spaces on S (which is a smooth contour for 2D). This affiliation of the total fields necessitates their Fourier coefficients obey $\sum_{m=-\infty}^{\infty} \left|\varpi_{i,m}^{\pm}\right|^2 [1+|m|]^{\pm 1} < \infty$ [27], i.e. they decay or grow faster than $\sqrt{m}, m \to \infty$. On the other hand, the Fourier coefficients of the Green function on S - $W_m^{(\iota_i)}(k_i a)$ contribute to λ_m^i with the radial eigen-functions (Bessel and Hankel functions of integer degree) written in the null-fields and prime stands for the derivative with respect to argument. Let s=±1, plus for standing waves and minus for travelling waves and $\delta_{s,1}$ is 1 and 0, respectively, for the moment. The amplitude of the corresponding radial eigen-functions is asymptotically $W_m^{(s)}(t) \leq e^{s|Im(t)|}[(m-1)!]^{-s}(m)^{-\delta_{s,1}}\left|(t/2)^m\right|^s, m \to \infty$ [23, 27]. Apparently, λ_m^i in (4), accommodates the fast increase and decrease of $W_m^{(\iota_i)}(k_i a)$ more than that of $\varpi_i^{\pm}$ due to their asymptotic behavior as m increases. This perspective from 2D boundary integral representations reveals the dependence of the scattering and transmission coefficients of a circularly cylindrical dielectric system to the

radial eigen-functions. The path to the regularization of the corresponding T-matrices is formed through Rayleigh formulation via the regularizers that have the reciprocal asymptotic behavior with respect to these radial eigen-functions: $e^{-s|Im(t)|}\left[(m-1)!\right]^{s}(m)^{\delta_{s,1}}\left|(t/2)^{m}\right|^{-s}, m\to\infty$ [23, 27]. Let us rewrite $\boldsymbol{\alpha}/\mathbf{f}$ i.e. the standing/travelling eigen-function coefficients of the scattered field from a circular dielectric cylinder with a factorization exposing the fastly growing/decaying asymptotic behaviour of the radial eigen-function content in them which also defines the new unknown coefficients $\tilde{\boldsymbol{\alpha}}/\tilde{\mathbf{f}}$ and the isolated T-matrix equations they belong in Table 1:

Table 1. Linear algebraic equation systems (LAES) for the isolated scatterer.

Eigen-function for	Unknown	Isolated LAES$_i$	Regularizer pair	Isolated LAES$_w$
Standing waves	$\boldsymbol{\alpha}=\overline{\mathbf{R}}_{\alpha}\cdot\widetilde{\boldsymbol{\alpha}}$	$\overline{\mathbf{Q}}\cdot\boldsymbol{\alpha}=-i\mathbf{a}$	$(\overline{\mathbf{L}}_{\alpha},\overline{\mathbf{R}}_{\alpha})$	$\overline{\mathbf{L}}_{\alpha}\cdot\overline{\mathbf{Q}}\cdot\overline{\mathbf{R}}_{\alpha}\cdot\widetilde{\boldsymbol{\alpha}}=-i\overline{\mathbf{L}}_{\alpha}\cdot\mathbf{a}$
Travelling waves	$\mathbf{f}=\overline{\mathbf{R}}_{f}\cdot\widetilde{\mathbf{f}}$	$\overline{\mathbf{Q}}^{t}\cdot\mathbf{f}=-\Re\mathrm{e}\overline{\mathbf{Q}}^{t}\cdot\mathbf{a}$	$(\overline{\mathbf{L}}_{f},\overline{\mathbf{R}}_{f})$	$\overline{\mathbf{L}}_{f}\cdot\overline{\mathbf{Q}}^{t}\cdot\overline{\mathbf{R}}_{f}\cdot\widetilde{\mathbf{f}}=-\overline{\mathbf{L}}_{f}\cdot\Re\mathrm{e}\overline{\mathbf{Q}}^{t}\cdot\mathbf{a}$

In Table 1 we used the equation that leads to the same T-matrix through Rayleigh formulation for the travelling waves [7], also because it is the form used in [23] aside the one for standing waves both being consistent with the derivation of the result in (4). The definitions of the right hand regularizers of the infinite linear algebraic equation systems of the first kind which are ill-conditioned (LAES$_i$) for the T-matrix equations are also given in Table 1. This is the initial step for the application of the analytical regularization method (ARM) [22] which in turn applies to LAES$_i$ as in Table 1, i.e. $\overline{\mathbf{A}}\cdot\mathbf{x}=\mathbf{b},\quad \mathbf{x},\mathbf{b}\in l_2$ where l_2 is the space of sequences with sum of terms' squares is finite. The LAES$_i$ established for interaction of the circular dielectric cylinders are shown to be extremely ill-conditioned with respect to increasing truncation number [24]. The LAES$_w$ arrived at after ARM there possess uniformly bounded condition numbers and their solutions are exponentially converging with increasing truncation numbers. The ARM establishes the left and right hand side regularizer pair $\left(\overline{\mathbf{L}},\overline{\mathbf{R}}\right)$ for the LAES1 to lead to LAES2 $\left[\overline{\mathbf{I}}+\overline{\mathbf{K}}\right]\cdot\mathbf{y}=\mathbf{g}\quad \mathbf{y},\mathbf{g}\in l_2$. Here $\mathbf{x}=\overline{\mathbf{R}}\cdot\mathbf{y},\mathbf{g}=\overline{\mathbf{L}}\cdot\mathbf{b}$, and $\overline{\mathbf{K}}=\overline{\mathbf{L}}\cdot\overline{\mathbf{A}}\cdot\overline{\mathbf{R}}$ where $\overline{\mathbf{I}}$ is the identity and $\overline{\mathbf{K}}$ and $\overline{\mathbf{A}}$ are compact operators in l_2. These pairs of regularizers consisting of radial eigen-functions evaluated on circular boundary S are also addressed in Table 1 (see Appendix for the 2D implementation). For the cases in Table 1 the corresponding LAES$_w$'s are also addressed in Appendix. For an isolated circular cylindrical boundary these correspond to the analytical solutions of the scattering problem.

The performance of the ARM on the eigen-surfaces in T-matrix formulations inseminates the ideas on its applicability of it for the other surfaces during the corresponding scattering field calculations. It is not straightforward to achieve a formula like (4) for a surface other than the eigen-surface explicitly. Nevertheless, since the same eigen-function expansions of the fields are being exploited beyond the extended boundaries S_{i_i} in the null-fields, we can produce compatible suggestions for the regularization of the problem at hand on S_{i_i} to factorize our unknown coefficients for their fast growing or decaying. Our numerical experiments approved the following: With the intuition just presented and having the excitation performed in $V_i, i=1,2$, the pair $\left(\overline{\mathbf{L}}_{\alpha},\overline{\mathbf{R}}_{\alpha}\right)/\left(\overline{\mathbf{L}}_{f},\overline{\mathbf{R}}_{f}\right)$ can be defined on an extended circular boundary S_i/S_{i_i} of the scattering region V_{i_i}/V_i as if their parameters are valid throughout the shell region.

In the next section we will demonstrate the numerical results of the injection of the regularization outlined above with a variety of problems concerning an isolated dielectric scatterer. We will study the condition of the matrix $\overline{\mathbf{Q}}$ inverted in the relation $\boldsymbol{\alpha}=-i\overline{\mathbf{Q}}^{-1}\cdot\mathbf{a}$, that is critical.

3. Numerical results

Predicting the truncation number of the infinite LAES$_i$ solving for an isolated scatterer always requires a preprocess depending on the satisfaction of the boundary conditions (3) with a certain error. This error depends on the size of this scatterer and has to be controlled either by confirmation of boundary condition for each truncation or via usage of the empirical formulae [29]. The complexity of the latter during the multiple scattering calculations makes the satisfaction of the former critical. Even for eigen-surfaces as scatterers, the excess of the critical truncation number in the corresponding ill-conditioned LAES$_i$ (that a double precision environment can only shift it to its larger values rather than eliminating it) leads to noisy solutions introduced by severe round-off errors. But the well-conditioned LAES$_w$ provides all the precision that a computer can deliver as truncation numbers keep on increasing [23].

Here we elaborate on similar aspects during calculation of the scattering using T-matrix algorithm, from an arbitrary shaped object accounting its corrugation and elongation which erode the condition of the system. Even before detailing the numerical results setup we can apply to the help of Table 2 in order to develop the understanding of the condition characteristic before and after the regularization we employ, where we pick two excitation cases and illuminate pentagonal/tetragonal dielectric cylindrical boundary with low and high corrugation/elongation both at different electrical sizes, respectively. We witness single occurrence of regularization outcome as in eigen-surfaces as in [23] i.e. for the low level of corrugation of a pentagon, where the condition number of $< \overline{\mathbf{Q}} >$ - $< \overline{\mathbf{L}}_\alpha \cdot \overline{\mathbf{Q}} \cdot \overline{\mathbf{R}}_\alpha >$, i.e. before - after regularization is growing with acceleration - uniformly bounded respectively. When the pentagon is highly corrugated, even though we lose the uniform bound after regularization we have a better conditioned system than before its regularization. Keeping in mind that, roughly in a 16 decimal digit precision environment, the condition number of the levels 10^γ, provide (16 -γ) correct figure precision as $\gamma \geq 16$ would mean total loss of accuracy. Thus after the applied regularization we not only can extend the correct precision range for the truncation numbers but also can trace the direct effect of corrugation. We can draw exactly the same conclusions for highly elongated tetragon example much stronger and observe that we cannot exceed 15 as a truncation number for some correct decimal figures in the calculation where this number was 30 in previous example. Even for the low elongation case we witness that the regularization works for well-conditioning leading to a slow increase rather than uniform bound for the condition numbers. There are three reasons we can point for this behavior: (i) the polarization, (ii) the electrical size being larger than previous example, and (iii) exciting with line source inside meets concave boundaries, i.e. effective corrugation accompanies the low level of elongation. The third reason is more generalizable than the other two as a rule of thumb.

As has been built within the context of Table 2 and also pointed out in subsection 2.2., the regularizers described in Appendix established for a circularly cylindrical boundary [23] are specified here to the obstacle of arbitrary shape by setting its constant radius to that of the closest extended circular boundary in the nonnull (source) field region with the constitutive parameters of the null-field region. We discuss the validity of the suggested regularization and its well-conditioning the T-matrices of the excited with line source that can be situated outside or inside the isolated cylindrical object under 5 different corrugation and elongation levels modeled by an infinitely smooth parametrization in polar coordinates [28] (Figures 1B and 1C) of 5 different electrical sizes (for brevity, 3 of TM polarized and 2 of TE polarized are used among 5) upon the results in Figures 2–5. The definitions of source locations and size formations are below. Table 2 exploits other cases than those of Figures 2–5. The well-conditioned version of this algorithm with the formulae given in Appendix is used throughout these processes.

Table 2. Typical condition number behavior of the nonregularized and regularized-low/high level corrugated/elongated T-matrix algebraic systems.

Truncation number M	TE line source outside exciting pentagon with r_3=0.1λ_0 size (Figure 1B)			
	No corrugation - level 0		High corrugation - level 4	
	$LAES_i$	$LAES_w$	$LAES_i$	$LAES_w$
5	4.520726E+04	1.463209E+00	2.374010E+07	1.476931E+02
10	3.688527E+15	1.597232E+00	1.730765E+23	6.491989E+05
15	1.623003E+29	1.647045E+00	3.723354E+39	2.093149E+07
20	6.794381E+46	1.673941E+00	3.276547E+61	1.441523E+09
25	3.339624E+62	1.690682E+00	2.388575E+79	1.081758E+12
30	1.291599E+78	1.701773E+00	8.276802E+95	1.699688E+14
35	5.342410E+92	1.709357E+00	1.353189E+113	2.121259E+16
40	1.706067E+106	1.714623E+00	2.107318E+128	7.331803E+18
45	2.141027E+121	1.718299E+00	1.909644E+146	1.824876E+23
50	3.256766E+136	1.720863E+00	1.033283E+164	6.051799E+28
Truncation number M	TM line source inside exciting tetragon with r_4=0.5λ_0 size (Figure 1C)			
	No elongation - level 0		High elongation - level 4	
	$LAES_i$	$LAES_w$	$LAES_i$	$LAES_w$
5	2.342328E+00	4.822262E+00	9.360798E+01	1.182854E+03
10	2.036235E+03	4.974743E+01	1.453967E+04	9.821883E+08
15	4.363847E+06	6.147461E+01	1.038366E+07	9.052588E+13
20	9.429246E+11	8.366477E+01	3.586011E+10	9.231106E+18
25	1.855299E+19	2.197917E+02	1.127861E+17	5.459557E+24
30	3.868848E+27	9.369490E+02	1.120411E+30	1.965060E+30
35	1.652012E+37	8.341208E+03	1.763890E+42	3.346918E+34
40	1.350175E+47	8.486358E+04	1.113437E+57	6.786387E+36
45	1.445377E+59	1.135594E+06	8.136292E+69	4.285280E+40
50	1.345394E+70	1.342509E+07	3.113532E+82	3.222684E+43

With the parameters to be defined in next paragraph on below, the infinitely smooth boundary of 2D isolated scatterer of relative permittivity $\varepsilon_r = 4$ situated in free-space ($\varepsilon_r = 1$) is parameterized using (7), choosing $\epsilon_{1,2} = 0$. Such arrangements for (7) are critical not only working out the conditioning of the T-matrix method weakening with the corrugation and elongation of the boundaries but also for the superalgebraic convergence of the BIE solver in [10] used for benchmark.

The line source emitting waves of length λ_0 is either situated to the central coordinates to each contour i.e. (x_c, y_c), or in the center of the global coordinates $0.5\lambda_0$ far from the leftmost nearest point of the scatterer along the horizontal axis. The aforementioned different electrical sizes are scaled with the usage of the parameter r exploited below defined as $r_i = t_i\lambda_0$ where $t_1 = 0.01, t_2 = 0.05, t_3 = 0.1, t_4 = 0.5, t_5 = 1$.

With $a = b = 1, m = 5, n_{2,3} = 60$, choosing $n_1 \in \{100, 80, 60, 40, 20\}$ (7) corrugates the pentagon to a star in five steps. Here (7) is normalized by its maximum before scaling it with r to electrical dimension preserving the circumscribing circle radius to be r: $r \times \rho(\varphi)/max(\rho(\varphi)), \varphi \in (-\pi, \pi]$ in Figure 1B.

Setting $a \in \{1, 1.25, 1.5, 1.75, 2\} = 1/b, m = 4, n_{1,2,3} = 30$, (7) elongates the rectangle in five steps where its scaling to the electrical dimension is performed with $r \times \rho(\varphi), \varphi \in (-\pi, \pi]$ preserving its area in Figure 1C to λ^2.

The –abscissa,ordinate– pair of local frames for Figures <2-3> and <4-5> are the truncation numbers of the algebraic systems and from none to high, 5 levels of <corrugation-elongation>, respectively.

The ordinates of global frames for Figures <2-3> and <4-5> are samples from the used line source excitation where the 5 row bottom-up line up has $r_{2,4}$ for TE and $r_{1,3,5}$ for TM cases picked for brevity among 5 levels of obstacle sizes and two different polarizations. Each consecutive pair of the abscissas of 4 columns of global frames present data when the line source is placed outside and inside, respectively.

Let the relative l_2 norm of Y with respect to X be abbreviated as follows: $\lfloor Y, X \rfloor_2 = \|X - Y\|_2 / \|X\|_2$. This is equivalent to relative version of root mean square (RMS) deviation of Y from X. All the relative errors of Y with respect to X are calculated using this formula in the definition of figures below.

The abscissas of each consecutive pair of 4 columns of global frames for Figures <2-3> stand for relative errors for the scattered field values observed on the extended cylindrical boundary C_{1-2} (similar to S_{1-2} in Figure 1A), respectively. First/second of these pairs present a comparison of values obtained via LAES$_w$/LAES$_i$ w.r.t. the BIE method in [10]/LAES$_w$ explained in this work. The physical relevance of the results that LAES$_w$ provides is clearly traceable in the comparisons made with BIE at a large enough truncation number especially when corrugation or elongation is not increased to a certain level. These results exhibit large deviations from that of LAES$_i$ as truncation number increases as well as the effect of elongation and corrugation does.

The abscissas of 4 columns of global frames for Figures <4-5> bear data of the condition number of the regularized matrix $\overline{\mathbf{L}}_\alpha \cdot \overline{\mathbf{Q}} \cdot \overline{\mathbf{R}}_\alpha$ and relative error of the coefficients $\boldsymbol{\alpha}_i$ obtained via the relation $\boldsymbol{\alpha}_i = -i\overline{\mathbf{Q}}^{-1} \cdot \mathbf{a}$ w.r.t coefficients $\boldsymbol{\alpha}_w$ where $\boldsymbol{\alpha_w} = \overline{\mathbf{R}}_\alpha \cdot \widetilde{\boldsymbol{\alpha}}$ both defined in Table 1. Working only with these transmission coefficients ($\boldsymbol{\alpha}$) to save space contents us since their characteristics before and after regularization reflect parallel features with that of the reflection coefficients ($\mathbf{f} = -\Re\mathfrak{e}\overline{\mathbf{Q}} \cdot \overline{\mathbf{Q}}^{-1} \cdot \mathbf{a} = -\left[\overline{\mathbf{Q}}^t\right]^{-1} \cdot \Re\mathfrak{e}\overline{\mathbf{Q}}^t \cdot \mathbf{a} = \overline{\mathbf{R}}_f \cdot \widetilde{\mathbf{f}}$) based on the expressions in subsection 2.1 and Table 1. These transmission coefficients also exhibit large deviations before and after regularization agreeing on a few initial coefficients only, which are due to the ill-conditioned nature of LAES$_i$ tabulated with accelerated increase of their condition numbers in Table 2. On the contrary the condition numbers of LAES$_w$ here exhibit much predictably increasing character owing to the increasing elongation and corrugation. When effects of these are coming in sight the condition number exhibits a regulated version of the increase before the regularization. Otherwise a uniform bound for the condition number behavior with increasing truncation is observed. We understand that the applied regularization based on the extended circular boundary is sufficient for these latter cases while for the former ones they do not fully and there is still a room for further improvement. Recall the statement about 16 decimal digit precision environment above during evaluation of Table 2 above reading these tables. We can conclude that after applying the suggested regularization we can reach to solutions with much more amount of significant digits than before its application providing an error controlling mechanism.

The condition numbers of the LAES$_b$ [18] have been of concern and left out of the figures presented for brevity where this system was regularized using the mean radius of (7) as applied in [18]. They have indicated a well conditioning of the system but the suggested version here is a better performance.

4. Conclusion

We introduced a well-conditioning strategy for the T-matrix algorithm exemplified on a cylindrical isolated dielectric scatterer of arbitrary cross section. Its inevitable native weakness i.e. the geometrical ill-conditioning effects of increasing corrugation and elongation of these cross sections became numerically traceable with this

novel strategy that reduces the capacity for potential round-off errors through the applied regularization on the circular extended boundaries in the counter null-fields. A superalgebraically convergent boundary integral equation formulation is taken as benchmark solver under excitation of a line source both from inside and outside the chosen variety of boundaries demonstrating the physical relevance of the obtained new results. Regarding the regularization of the multiple scattering of circular boundaries, we can forecast straightforwardly that the new well-conditioning has a large potential to be effective for the T-matrix algorithm for multiple scatterers we will investigate in a future work thoroughly.

5. Appendix

In this section we cast the necessary formulae for the algorithm specified to 2D problems both for the cases of excitation by a line source residing in the regions of either open background or the closed in-dielectric. The notation is compatible with Table 1. The fields the line source excites and all the scattering fields are longitudinal electric/magnetic fields which are TM/TE polarized with constitutive parameter p below standing for permeabilities(μ)/permittivities(ε), respectively.

The addition theorem for travelling wave cylindrical harmonics is the central formula and forms a base to various aspects of integral equation formulations [16, 23]

$$H_m^{(2)}\left(k_i\left|\boldsymbol{\rho}-\boldsymbol{\rho'}\right|\right)e^{jm\varphi''}=\sum_{n=-\infty}^{\infty}\begin{bmatrix}J_{n-m}\left(k_i\rho'\right)H_n^{(2)}\left(k_i\rho\right) & ;\rho>\rho'\\ H_{n-m}^{(2)}\left(k_i\rho'\right)J_n\left(k_i\rho\right) & ;\rho<\rho'\end{bmatrix}e^{jn\varphi-j(n-m)\varphi'}. \tag{5}$$

Note that (5) encapsulates the standing wave cylindrical harmonics only by substituting J instead of $H^{(2)}$ everywhere in the formula. The Green's function of the two dimensional Helmholtz equation has the following expansion in cylindrical harmonics using (5):

$$g_i\left(\boldsymbol{\rho},\boldsymbol{\rho'}\right)=-\frac{j}{4}H_0^{(2)}\left(k_i\left|\boldsymbol{\rho}-\boldsymbol{\rho'}\right|\right)=-\frac{j}{4}\sum_{n=-\infty}^{\infty}J_n\left(k_i\rho_<\right)H_n^{(2)}\left(k_i\rho_>\right)e^{jn\left(\varphi-\varphi'\right)};\quad \rho_<<\rho_>. \tag{6}$$

Entries of the matrix $\overline{\mathbf{Q}}$ for the 2D problem integrated on the modified superformula contours C with the parametrizations in (7) [28]

$$\rho\left(\varphi\right)=\left[\left[\sqrt{cos^2\left(m\varphi/4\right)+\epsilon_1^2}/a\right]^{n_2}+\left[\sqrt{sin^2\left(m\varphi/4\right)+\epsilon_2^2}/b\right]^{n_3}\right]^{-1/n_1} \tag{7}$$

adjusted according to the given settings in Section 3, integral on which assumes $\int_C dC'=\int_{-\pi}^{\pi}d\varphi'\dot{\rho}'\left(\varphi'\right)$

$$Q_{nm}=-\frac{j}{4}\int_{-\pi}^{\pi}d\varphi'\dot{\rho}'\left(\varphi'\right)\begin{bmatrix}\left\langle H_n^{(2)}\left(k_i\rho'\left(\varphi'\right)\right)e^{-jn\varphi'}\right\rangle\hat{n}\cdot\nabla'\left\langle J_m\left(k_{\imath_i}\rho'\left(\varphi'\right)\right)e^{jm\varphi'}\right\rangle p_{\imath_i}/p_i\\ -\left\langle J_m\left(k_i\rho'\left(\varphi'\right)\right)e^{jm\varphi'}\right\rangle\hat{n}\cdot\nabla'\left\langle H_n^{(2)}\left(k_{\imath_i}\rho'\left(\varphi'\right)\right)e^{-jn\varphi'}\right\rangle\end{bmatrix}. \tag{8}$$

The expansion coefficients $\boldsymbol{\alpha}$ and $\mathbf{f}$ of the transmitted and the scattered field excited from $<outside, inside>$ $(i=<1,2>)$ with the incident field of a line-source at $\boldsymbol{\rho'}=(\rho',\varphi')$ with the expansion coefficients $\mathbf{a}=\left[\left\langle H_n^{(2)},J_n\right\rangle\left(k_i\rho'\right)e^{-jn\varphi'}\right]_{n=-\infty}^{\infty}$ where vector of cylindrical harmonics for {standing, outgoing} waves

$\{\mathbf{S},\mathbf{O}\}(\boldsymbol{\rho}) = \left[\left\langle \{J_n, H_n^{(2)}\}, \{H_n^{(2)}, J_n\} \right\rangle (k_{\imath_i}\rho)\, e^{jn\varphi}\right]_{n=-\infty}^{\infty}$ enables following expressions: $\phi_{inc}(\boldsymbol{\rho}) = \mathbf{a}\cdot\mathbf{S}(\boldsymbol{\rho}), \phi_{tra}(\boldsymbol{\rho}) = \boldsymbol{\alpha}\cdot\mathbf{S}(\boldsymbol{\rho}), \phi_{sca}(\boldsymbol{\rho}) = \mathbf{f}\cdot\mathbf{O}(\boldsymbol{\rho})$. The right-hand side regularizers are written as diagonal matrices evaluated on the extended circular boundary of the nonnull-field region

$$\overline{\mathbf{R}}_\alpha = diag\left[H_n^{(1)}(k_i a_i)^{\langle -1,1\rangle}\right]_{n=-\infty}^{\infty}; \quad \overline{\mathbf{R}}_f = diag\left[H_n^{(1)}(k_i a_i)^{\langle 1,-1\rangle}\right]_{n=-\infty}^{\infty}. \tag{9}$$

Note that the $H_n^{(1)}$ or its reciprocal is used for the factorization of the asymptotic behaviours for coefficients $\boldsymbol{\alpha}$ and $\mathbf{f}$ instead of $H_n^{(2)}$ and J_n, respectively. Because $H_n^{(1)}$ imposes its zeros on the phasors which are in the Riemann sheet that is impossible to meet within the time-harmonic regime of the problem [23]. With (10) below and the diagonal entries of the matrix $\overline{\mathbf{Q}}$ for circle of radius a_i being defined as the diagonal matrix $\mathbf{P}$

$$\mathbf{P} = diag\left[-\frac{j\pi a_i}{2}\left\langle H_n^{(2)}(k_i a_i)\,\hat{n}\cdot\nabla' J_n(k_{\imath_i} a_i)\frac{p_{\imath_i}}{p_i} - J_n(k_i a_i)\,\hat{n}\cdot\nabla' H_n^{(2)}(k_{\imath_i} a_i)\right\rangle\right]_{n=-\infty}^{\infty} \tag{10}$$

we can define the left-hand side regularizers for transmission and reflection T-matrices in Table 1 [23] as $\overline{\mathbf{L}}_\alpha = \overline{\mathbf{R}}_\alpha^{-1}\cdot\mathbf{P}$ and $\overline{\mathbf{L}}_f = \overline{\mathbf{R}}_f^{-1}\cdot\mathbf{P}$.

References

[1] Yuan SSA, Lin ZH, Lv L-B, Hao S-J, Sha WEI. Investigating the Scattering Characteristics of Artificial Field-Aligned Irregularities Based on T-matrix Algorithm. IEEE Journal on Multiscale and Multiphysics Computational Techniques (Early Access) 2023; 1-11. doi:10.1109/JMMCT.2023.3252053

[2] Theobald D, Beutel D, Borgmann L, Mescher H, Gomard G et al. Simulation of light scattering in large, disordered nanostructures using a periodic T-matrix method. Journal of Quantitative Spectroscopy and Radiative Transfer 2021; 272: 107802. doi:10.1016/j.jqsrt.2021.107802

[3] Hu S, Liu L, Zeng Q, Gao T, Zhang F. An investigation of the symmetrical properties in the invariant imbedding T-matrix method for the nonspherical particles with symmetrical geometry. Journal of Quantitative Spectroscopy and Radiative Transfer 2021; 259: 107401. doi:10.1016/j.jqsrt.2020.107401

[4] Scattering T-matrix Codes, Electromagnetic Scattering by Particles and Surfaces. NASA GISS: Database of T-Matrix Publications.

[5] Mishchenko MI. Comprehensive thematic T-matrix reference database: a 2017–2019 update. Journal of Quantitative Spectroscopy and Radiative Transfer 2020; 242: 106692. doi:10.1016/j.jqsrt.2019.106692

[6] Harrington RF. Boundary Integral Formulations for Homogeneous Material Bodies. Journal of Electromagnetic Waves and Applications 1989; 3 (1): 1-15. doi:10.1163/156939389X00016

[7] Chew WC. Waves and Fields in Inhomogenous Media. IEEE 1995; 429-509. doi:10.1109/9780470547052.ch8

[8] Pao Y-H. Betti's identity and transition matrix for elastic waves. The Journal of the Acoustical Society of America 1978; 64: 302-310. doi:10.1121/1.381986

[9] Yeh Y-K, Pao Y-H. On the transition matrix for acoustic waves scattered by a multilayered inclusion. The Journal of the Acoustical Society of America 1987; 81: 1683-1687. doi:10.1121/1.394781

[10] Sever E, Dikmen F, Tuchkin YA. Superalgebraically converging Galerkin method for electromagnetic scattering by dielectric cylinders. Radio Science 2017; 52: 1282-1292. doi:10.1002/2017RS006328

[11] Chen J-T, Kao J-H, Kao S-K, Shao C-H, Tai W-C. On the role of singular and hypersingular BIEs for the BVPs containing a degenerate boundary. Engineering Analysis with Boundary Elements 2021; 133: 214-235. doi:10.1016/j.enganabound.2021.07.018

[12] Chew WC, Michielssen E, Song JM, Jin JM. Fast and Efficient Algorithms in Computational Electromagnetics. Artech House, Inc, 2001.

[13] Gürel L, Chew WC. A recursive T-matrix algorithm for strips and patches. Radio Science 1992; 27 (3): 387–401. doi:10.1029/91RS03054

[14] Hafner C. Chapter 3 - The Multiple Multipole Program (MMP) and the Generalized Multipole Technique (GMT). In: Wriedt T (editor). Mechanics and Mathematical Methods–Series of Handbooks, Generalized Multipole Techniques for Electromagnetic and Light Scattering, Elsevier Science B.V., 1999, pp. 21-38. doi:10.1016/B978-044450282-7/50015-4

[15] Bogdanov FG, Karkashadze DD, Zaridze RS. Chapter 7 - The Method of Auxiliary Sources in Electromagnetic Scattering Problems. In: Wriedt T (editor). Mechanics and Mathematical Methods–Series of Handbooks, Generalized Multipole Techniques for Electromagnetic and Light Scattering, Elsevier Science B.V., 1999, pp. 143-172. doi:10.1016/B978-044450282-7/50019-1

[16] Lee Y-T, Kao J-H, Chou Y-T, Chen J-T. A systematic approach for potentials on closely packed cells using the null-field boundary integral equation in conjunction with the degenerate kernel and eigenfunction expansion. Engineering Analysis with Boundary Elements 2022; 140: 98-112. doi:10.1016/j.enganabound.2022.03.023

[17] Waterman PC. Symmetry, unitarity, and geometry in electromagnetic scattering. Physical Review D 1971; 3 (4): 825-839. doi:10.1103/PhysRevD.3.825

[18] Bolomey JC, Wirgin A. Numerical comparison of the Green's function and the Waterman and Rayleigh theories of scattering from a cylinder. Proceedings of the Institution of Electrical Engineers 1974; 121 (8): 794-804. doi:10.1049/piee.1974.0183

[19] Stout B, Auger JC, Devilez A. Recursive T matrix algorithm for resonant multiple scattering: applications to localized plasmon excitations. J. Opt. Soc. Am. A 2008; 25 (10): 2549-2557.

[20] Ivanov EA. Diffraction of Waves from Two Bodies (in Russian and Translated to English as NASA TT F-597). Nauka i Tekhnika, Minsk, 1968.

[21] Majic M. Relationships between spherical and bispherical harmonics, and an electrostatic T-matrix for dimers. Journal of Quantitative Spectroscopy and Radiative Transfer 2021; 276: 107945. doi:10.1016/j.jqsrt.2021.107945

[22] Tuchkin YA. On the analytical regularization method in scattering and diffraction. In: Kobayashi K, Smith PD (editors). Advances in Mathematical Methods for Electromagnetics, The ACES series on Computational Electromagnetics and Engineering, Institution of Engineering and Technology (IET) 2020, pp. 303-328. doi:10.1049/SBEW528E_c

[23] Dikmen F, Sever E, Vatansever S, Tuchkin YA. Well-conditioned algorithm for scattering by a few eccentrically multilayered dielectric circular cylinders. Radio Science 2015; 50: 99-110. doi:10.1002/2014RS005501

[24] Bates RHT. Analytic Constraints on Electromagnetic Field Computations. IEEE Transactions on Microwave Theory and Techniques 1975; 23 (8): 605-623. doi: 10.1109/TMTT.1975.1128639

[25] Vico F, Ferrando M, Greengard L, Gimbutas Z. The decoupled potential integral equation for time harmonic electromagnetic scattering. Communications on Pure and Applied Mathematics 2016; 69 (4): 771-812. doi:10.1002/cpa.21585

[26] Hsiao GC, Kleinmann RE. Mathematical foundations for error estimation in numerical solutions of integral equations in electromagnetics. IEEE Transactions on Antennas and Propagation 1997; 45 (3): 316-328. doi:10.1109/8.558648

[27] Abramowitz M, Stegun IA. Handbook of Mathematical Functions with Formulas, Graphs, and Mathematical Tables. New York: Dover, 1964.

[28] Güler S, Önol C, Ergül Ö, Sever E, Dikmen F et al. Modified superformula contours optimized via genetic algorithms for fastly converging 2D solutions of EFIE. IEEE Antennas and Propagation Society International Symposium (APSURSI) Proceedings; 2016. pp. 1461–1462

[29] Neves AAR, Pisignano D. Effect of finite terms on the truncation error of Mie series. Optics Letters 2012; 37 (12): 2418. doi:10.1364/OL.37.002418

6. Appendix

In this section we cast the necessary formulae for the algorithm specified to 2D problems both for the cases of excitation by a line source residing in the regions of either open background or the closed in-dielectric. The notation is compatible with Table 1. The fields the line source excites and all the scattering fields are longitudinal electric/magnetic fields which are TM/TE polarized with constitutive parameter p below standing for permeabilities(μ)/permittivities(ε), respectively.

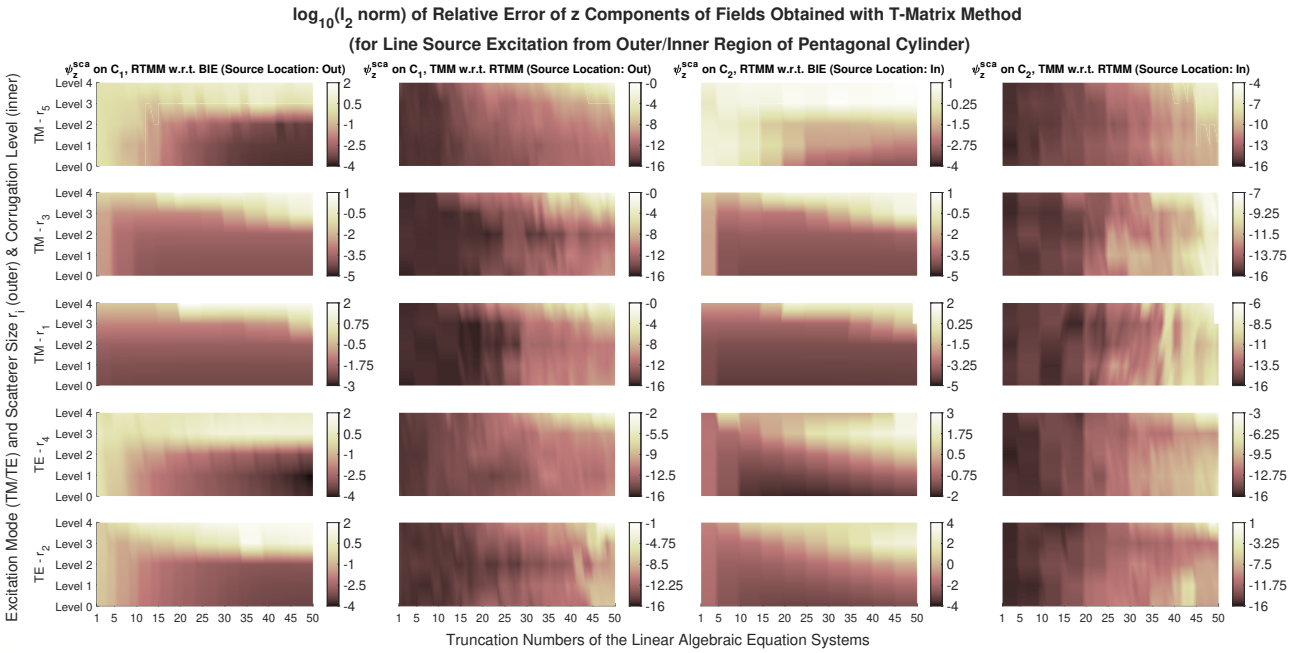

Figure 2. Plots w.r.t. increasing truncation number of the algebraic systems regarding the relative error of the z component of electric (TM)- magnetic (TE) scattered fields from the dielectric pentagon of electrical sizes $\mathrm{r}_{1,3,5}^{TM} = (0.01, 0.1, 1)\lambda_0$ - $\mathrm{r}_{2,4}^{TE} = (0.05, 0.5)\lambda_0$ at rows (1-3)–(4-5) measured on the extended boundary. The excitation with a line source outside - inside are worked out at columns (1-2)–(3-4) with 5 steps of corrugation (Figure 1B) from levels 0 to 4. The relative errors in columns (1,3) and (2,4) belong to (the regularized T-matrix method w.r.t. the BIE in [10]) and (traditional T-matrix method w.r.t the regularized one), respectively.

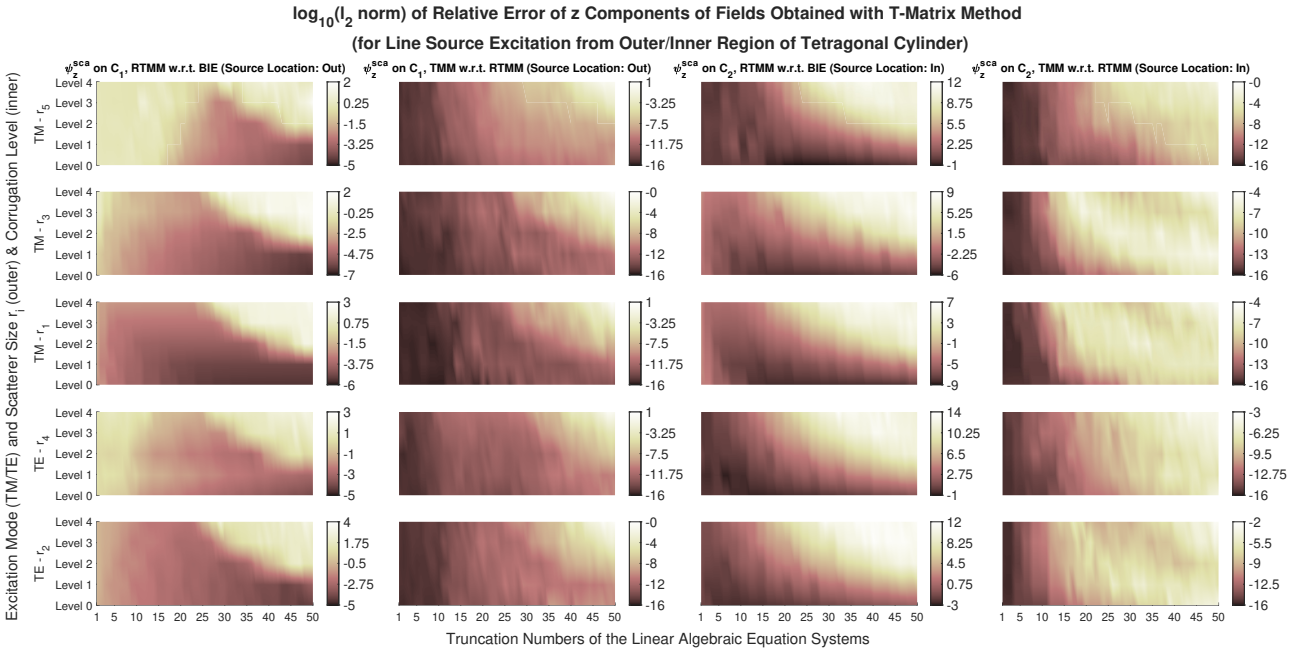

Figure 3. Plots w.r.t. increasing truncation number of the algebraic systems regarding the relative error of the z component of electric (TM)- magnetic (TE) scattered fields from the dielectric tetragon of electrical sizes $\mathrm{r}^{TM}_{1,3,5} = (0.01, 0.1, 1)\lambda_0$ - $\mathrm{r}^{TE}_{2,4} = (0.05, 0.5)\lambda_0$ at rows (1-3)–(4-5) measured on the extended boundary. The excitation with a line source outside - inside are worked out at columns (1-2)–(3-4) with 5 steps of corrugation (Figure 1C) from levels 0 to 4. The relative errors in columns (1,3) and (2,4) belong to (the regularized T-matrix method w.r.t. the BIE in [10]) and (traditional T-matrix method w.r.t the regularized one), respectively.

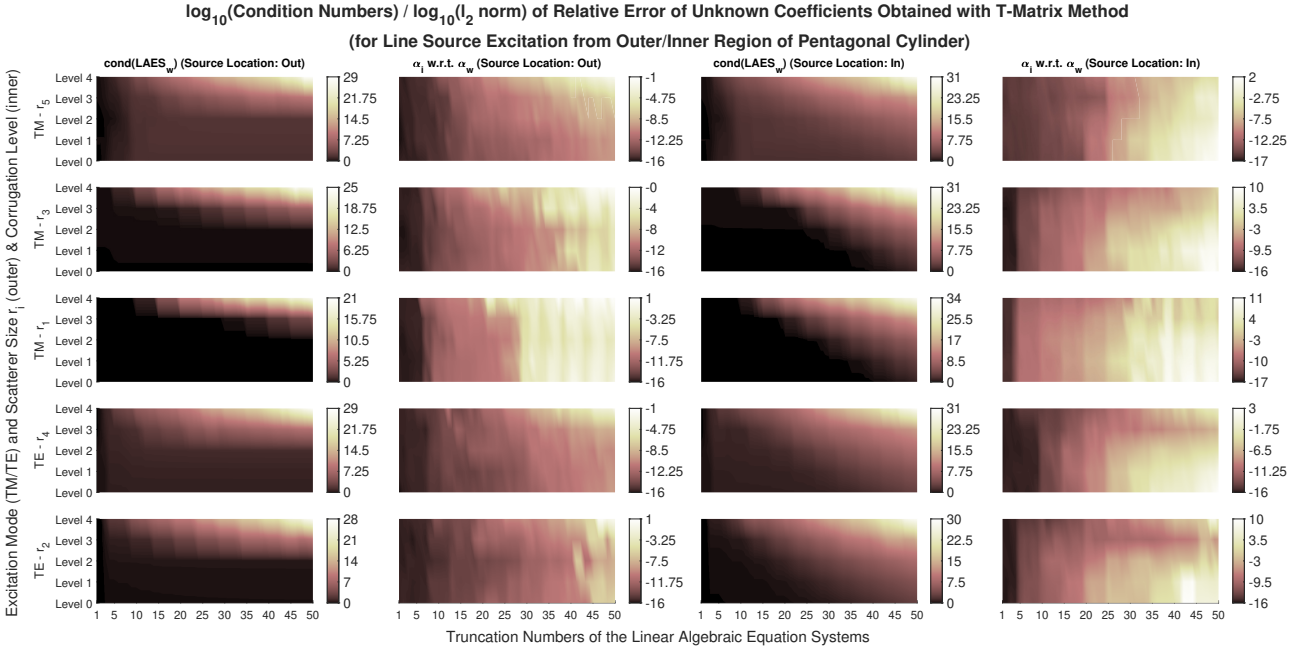

Figure 4. Plots w.r.t. increasing truncation number of the algebraic systems regarding the condition numbers of the LAES_w at columns (1,3) and relative errors of the solution vectors LAES_i provide w.r.t. solution vectors LAES_w provide at columns (2,4) used for the excitation scenarios in Figure 2 with 5 steps of corrugation (Figure 1B) from levels 0 to 4.

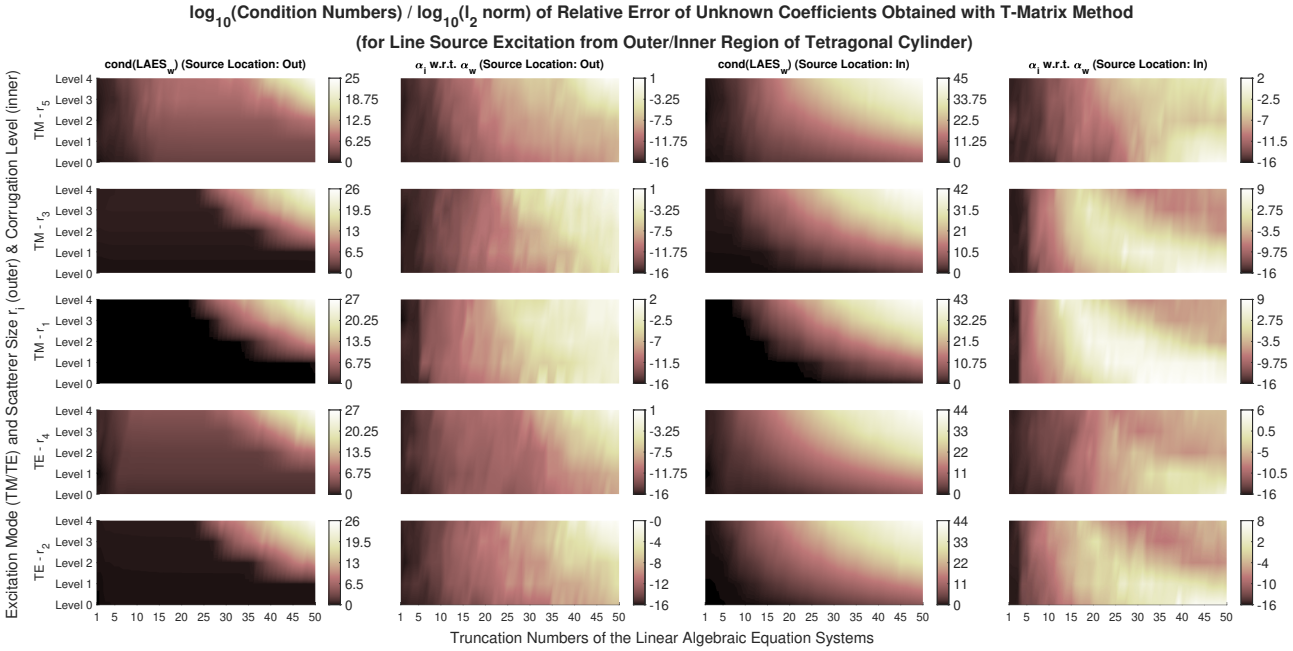

Figure 5. Plots w.r.t. increasing truncation number of the algebraic systems regarding the condition numbers of the LAES_w at columns (1,3) and relative errors of the solution vectors LAES_i provide w.r.t. solution vectors LAES_w provide at columns (2,4) used for the excitation scenarios in Figure 3 with 5 steps of corrugation (Figure 1C) from levels 0 to 4.